frontiers | Frontiers in Earth Science

TYPE Original Research
PUBLISHED 27 February 2024
DOI 10.3389/feart.2024.1269753

OPEN ACCESS

EDITED BY
Giovanni Martinelli,
National Institute of Geophysics and Volcanology, Italy

REVIEWED BY
Huai Zhang,
University of Chinese Academy of Sciences, China
Caibo Hu,
University of Chinese Academy of Sciences, China

*CORRESPONDENCE
Guofu Luo,
luoguofu_05@163.com

RECEIVED 30 July 2023
ACCEPTED 09 February 2024
PUBLISHED 27 February 2024

CITATION
Luo G, Xu Y, Luo H, Ding F and Li W (2024), Spatio-temporal characteristics of seismic strain anomalies reveal seismic risk zones along the Longmenshan fault zone and adjacent areas.
Front. Earth Sci. 12:1269753.
doi: 10.3389/feart.2024.1269753

Spatio-temporal characteristics of seismic strain anomalies reveal seismic risk zones along the Longmenshan fault zone and adjacent areas

Guofu Luo*, Yingcai Xu, Hengzhi Luo, Fenghe Ding and Wenjun Li

Seismological Bureau of Ningxia Hui Autonomous Region, Yinchuan, China

Introduction: Identifying and quantifying earthquake precursors, and analyzing their physical mechanisms, continues to be a challenge for earthquake forecasting. In this study, orthogonal functions were developed to effectively identify precursor anomalies, thereby improving the forecasting of strong earthquakes.

Methods: To study the spatio-temporal contour anomalies in seismic strain fields, we assessed them for seismic activity variables and natural orthogonal function expansion, in six strong earthquakes near the Longmenshan Fault Zone, China, that have occurred since 2008.

Results: We observed that, prior to these earthquakes, the temporal factor (the time variation characteristics of the strain field) displayed anomalies with high/low values exceeding the mean square error within a stable context. The anomalies exhibited multi-component characteristics and were primarily concentrated in the first four-strain fields. Short-term and impending-earthquake anomalies were observed in the temporal factor before the 2008 Wenchuan (*M*8.0) and 2013 Lushan (*M*7.0) earthquakes, while medium-term and long-term anomalies appeared before the other four strong earthquakes, without notable short-term anomalies. The temporal evolution of strain field contour anomalies, and the strain contours positive and negative intersection, showed that central areas surrounded by multiple strain field contour anomalies were potential locations for strong earthquakes. This suggests a potential approach for earthquake location forecasting. Since 2009, there have been five strong earthquakes, each affected to varying degrees by anomalous strain fields from the 2008 Wenchuan (*M*8.0) earthquake.

Conclusion: The results of this study corroborate the findings of the focal mechanism's node shear stress, indicating significant physical implications of the anomalies and the reliability of these conclusion.

KEYWORDS

Longmenshan fault zone, natural orthogonal function, seismic strain anomalies, temporal and spatial characteristics, shear stress results of focal mechanism

1 Introduction

The Longmenshan Fault Zone (LFZ) is situated in Sichuan Province, western China, where the eastern edge of the Tibetan Plateau converges with the Sichuan Basin. It has an approximate northeast (NE)–southwest (SW) orientation, spanning 500 km in length and 30–50 km in width. The NE end intersects with the Qinling Fault Zone, while the SW section obliquely intersects the Xianshuihe Fault Zone. The LFZ boasts a complex geological structure, comprising four main faults; the Houshan, Zhongyang, Qianshan, and Shanqianyinfu faults, and the associated thrusts (Chen et al., 2007; Li et al., 2008; Yi et al., 2012; Chen et al., 2013; Yang et al., 2021). The LFZ is bounded by the Bayankala block in the west and the Sichuan Basin in the east. The landform contrast between the mountains and basin is strong, and the topographic elevation difference within 50 km is approximately 4,000 m is an orogenic belt with obvious variation of terrain gradient and tectonic stress concentration (Deng et al., 1994; Fu et al., 2008; Yan et al., 2014; Shi and Gao, 2010); however, the average shortening rate under long-term evolution is not significant (Clark and Royden, 2000; Burchfield et al., 2008; Wang et al., 2017). Owing to the collision and extrusion of the Eurasian and Indian Ocean plates have led to an arc-shaped Himalayan orogeny thrusting into the northeastern margin of the Tibetan Plateau (Molnar and Tapponnier, 1975; England and Houseman, 1986; England and Houseman, 1988; Harrison et al., 1992; Fu et al., 2008; Luo et al., 2019). This resulted in an eastward drift of the Tibetan Plateau, which encounters substantial obstruction from the South China Block (Teng et al., 2014), leading to intense activity and deformation of LFZ structure and Bayan Har Block (Xu et al., 2008; Xu et al., 2013), consequently generating multiple strong earthquakes (Deng et al., 1994; Yang et al., 1999). The LFZ has therefore emerged as a significant focal point for research.

Before 2008, there were few earthquakes with a magnitude of *M*7 or higher on the LFZ, and the intensity of seismic activity was significantly lower than that of the Xianshuihe Fault Zone (towards the west) and the Minjiang Fault Zone (towards the north). However, on 12 May 2008, the Wenchuan earthquake (*M*8.0) took place in the midsection of LFZ, which was historically recognized for its lower seismic intensity (Yi et al., 2012; Gong et al., 2020). This earthquake caused a unilateral rupture in the northeast direction (Xu et al., 2008; Xu et al., 2009; Xu et al., 2010), with an approximate length of 340 km along the Zhongyang and Shanqian faults (Zhang et al., 2009).

Several studies have investigated patterns in the crustal strain field based on drilling experiments in seismogenic structures to provide different explanations for the generation and interaction of the Wenchuan (*M*8.0) earthquake (Zhang et al., 2008; Chen et al., 2013; Li et al., 2013; Wu et al., 2015; Li et al., 2016; Ye et al., 2017; Zheng et al., 2017; Li et al., 2018; Xu et al., 2018). Subsequently, on 20 April 2013, 5 years after the Wenchuan earthquake, the Lushan (*M*7.0) earthquake occurred on a blind thrust fault of southern LFZ (Xu et al., 2013; Li et al., 2014). This earthquake caused a rupture that was approximately 30 km long (Xie et al., 2018). The aftershock sequence of the Lushan earthquake (Zhao et al., 2013; Liu et al., 2019) and stress field inversion of the focal mechanism (Ma et al., 2021) provided evidence for the process of surface rupture. Many seismologists believe that the 2008 Wenchuan (*M*8.0) earthquake influenced the subsequent Lushan (*M*7.0) earthquake (Du et al., 2013; Wang et al., 2013; Yi et al., 2016; Jia and Zhou, 2018; Duan et al., 2020), and there has been extensive debate regarding the possibility of strong earthquakes occurring in a 50–60-km seismic gap between the area of influence of the two earthquakes (Wan et al., 2017; Diao et al., 2018; Guo et al., 2020; Li et al., 2022). In addition, a *M*6.6 earthquake occurred on the Lintan–Tanchang Fault, at the junction of Min and Zhang Counties in Gansu Province, which may have also been affected by the Wenchuan (*M*8.0) earthquake in 2008 (Ge, 2013; Huang et al., 2019). On 22 November 2014, the Kangding (*M*6.3) earthquake occurred in the southern Xianshuihe Fault Zone at the intersection with LFZ (Yi et al., 2015), which was triggered by Wenchuan (*M*8.0) and Lushan (*M*7.0) earthquakes (Wang et al., 2016). On 8 August 2017, the Jiuzhaigou (*M*7.0) earthquake occurred between the Minjiang and Tazang faults in the Shuzheng Fault Zone which lies north of LFZ. Research on the seismogenic fault, coseismic deformation field, and stress and strain states of the Jiuzhaigou earthquake (Shan et al., 2017; Xu et al., 2017; Cheng et al., 2018; Jin et al., 2019) explains the influence of the Wenchuan (*M*8.0) earthquake (Huang et al., 2019). After the Jiuzhaigou (*M*7.0) earthquake, stress in the vicinity of LFZ was effectively alleviated; however, stress in the Xianshuihe Fault Zone became acutely concentrated, resulting in a heightened possibility of strong earthquakes (Li et al., 2018). Consequently, the *M*6.8 Luding earthquake occurred in the Xianshuihe Fault Zone on 5 September 2022 (Li et al., 2022).

In summary, the Wenchuan (*M*8.0) earthquake led to changes in the stress state near LFZ, which affected seismic activity in the region. Over a span of 15 years, the 6 significant earthquakes described above occurred in the vicinity of LFZ. This study investigates the mutual interactions and influences between these strong earthquakes, focusing on the stresses released by each seismic event.

Several methods have been employed to investigate the interactions among strong earthquakes near LFZ. These methods can be categorized as follows: 1) Coulomb stress transfer analysis, which examines stress changes in different media or faults induced by strong earthquakes (Wan et al., 2009; Wang et al., 2014; Wang et al., 2014; Jin et al., 2019; Jia, 2020); 2) numerical simulations that model regional stress changes based on various hypocenter models (Toda et al., 2008; Shi and Cao, 2010; Yi et al., 2013); 3) focal mechanism solutions, in association with GPS and InSAR inversion, to assess regional stress variations (Yi et al., 2012; 2015; 2017; Jiang et al., 2014; Huang et al., 2019; Meng et al., 2022); and 4) calculation of regional stress changes by analyzing the stress and strain fields released during earthquakes (Luo et al., 2011; Yang and Ma, 2011; Yang and Ma, 2012; Luo et al., 2014; Luo et al., 2015; Yang et al., 2017; Luo et al., 2019; Luo et al., 2023).

The first three methods involve inversion models for computing regional stress changes. While these methods are well-established, they rely on various assumptions that can yield inconsistent results regarding stress effects. Consequently, their effectiveness continues to be a controversial topic. In contrast, the fourth method is a relatively recent development with fewer documented applications. In the present study, this fourth method was applied, utilizing the stress released by earthquakes in the vicinity of LFZ as the independent variable. Additionally, the natural orthogonal function (Neha and Pasari, 2022) was applied to investigate the

spatio-temporal variations in the regional strain field prior to the six powerful earthquakes with magnitudes ≥ $M6.3$ that have occurred since 2008. By identifying anomalous seismic activity preceding these events and analyzing the interactions and mutual influence among the earthquakes, this study offers new seismological insights into the seismic hazard and dynamic mechanisms of LFZ.

2 Methods and data

2.1 Methods

The natural orthogonal function (NOF) method is considered a cutting-edge tool for predicting, evaluating, and detecting small-scale, short-term, and long-term changes in datasets. This method is widely used in crustal deformation analysis and dimensionality reduction of data sets in seismological, climatic, and atmospheric sciences. Neha and Pasari, (2022) discusses the basic principles of the natural orthogonal function (EOF) method and its applications in various industries. Herein, we focus on how to use the natural orthogonal function method to extract temporal and spatial anomalies of seismic strain field before strong earthquakes.

The seismic strain field S, also called the natural orthogonal function expansion approach, was used to break down seismic strain (a random variable) into temporal and spatial functions (Luo et al., 2023). According to the intensity of seismic activity in the area, the strain field was constructed using the grid method for a particular study region.

The area was divided into n equal-area elements $\Delta S = \Delta x \times \Delta y$, with center coordinates of $\left(x_j, y_j\right)(j = 1, 2, ...n)$, and time interval Δt was selected. The observation time was divided into several m periods $t_i = \Delta t \times i(i = 1, 2, ...m)$. The derived and used as field function values reflecting the spatio-temporal coordinates $\left(x_i, y_i, t_j\right)(i, j = 1, 2, ...n)$ were set as the observed values for each area element in each time-period S_{ij}.

The release of seismic energy was symbolized by E. We considered the proportionality of the square root of seismic energy to seismic strain, i.e., $\sqrt{E} = c\varepsilon$ (Yang and Zhao, 2004), where c is the focal-related parameter of the earthquake in the study region and ε is the seismic focal region cumulative strain parameter, where both parameters reflect changes in the focal region's strain field. Following an evaluation of the area, the matrix form of the strain field function was established through $S = \sum_i \sqrt{E_i}$ (Yang and Ma, 2016) and expressed as follows:

$$\boldsymbol{S} = \begin{bmatrix} S_{11} & S_{12} & \cdots & S_{1m} \\ S_{21} & S_{22} & \cdots & S_{2m} \\ \vdots & \vdots & \vdots & \vdots \\ S_{n1} & S_{n2} & \cdots & S_{nm} \end{bmatrix} \tag{1}$$

Similar seismic blocks were present in the Longmenshan fault zone, and the seismic focal-related parameter c was almost constant. The seismic strain filed, also called the field function, where S_{ji} $(j = 1, 2, \ldots n, i = 1, 2, \ldots m)$ is the j-th time-period and i-th grid of the cumulative seismic strain value. The natural orthogonal function expansion approach was conducted by dividing the matrix S into the summation of the products of orthogonal spatial function X and orthogonal temporal function T (Yang and Ma, 2016):

$$S_{ji} = \sum_{k=1}^{n} T_{jk} X_{ki} \begin{cases} j = 1, 2, \cdots, n \\ i = 1, 2, \cdots, m \end{cases} \tag{2}$$

where X_{ki} is a spatial function that does not change with time and T_{jk} is a function of time that does not change in space. They satisfy the orthogonal and normalization conditions, respectively, as follows (Yang and Ma, 2016):

$$\sum_{i=1}^{m} X_{ki} X_{li} \begin{cases} 0 & k \neq l \\ 1 & k = l \end{cases} \tag{3}$$

$$\sum_{j=1}^{n} T_{jk} T_{jl} \begin{cases} 0 & k \neq l \\ 1 & k = l \end{cases} \tag{4}$$

The corresponding covariance matrix $R = S'S$ (Yang et al., 2017) characteristic equation is as follows:

$$\begin{bmatrix} R_{11} & R_{12} & \cdots & R_{1n} \\ R_{21} & R_{22} & \cdots & R_{2n} \\ \vdots & \vdots & \vdots & \vdots \\ R_{n1} & R_{n2} & \cdots & R_{nn} \end{bmatrix} \begin{bmatrix} x_1 \\ x_2 \\ \vdots \\ x_n \end{bmatrix} = \lambda \begin{bmatrix} x_1 \\ x_2 \\ \vdots \\ x_n \end{bmatrix} \tag{5}$$

The eigenvectors $\vec{x}_p$ and eigenvalues λ_p $(p = 1, 2, \ldots n)$ were obtained. Because the covariance matrix R is a real symmetric matrix, n eigenvalues are solved as positive real numbers. The physical meaning of the eigenvalues in this paper is to obtain the main strain field in the study area through a series of solutions. n eigenvalues correspond to n eigenvectors, which reflect the spatial characteristics of the strain field and are only spatial functions. The time factor of the strain field can be solved by the feature vector and the strain field, and the time-related anomalies of the seismic activity in the study area can be extracted by projection of the characteristics of the strain field over time.

The temporal factor of the strain field was expressed as (Yang and Ma, 2016):

$$\overrightarrow{T_p} = S\vec{x}_p \; p = 1, 2, \ldots n \tag{6}$$

The strain fields of eigenvectors $\vec{x}_p$ represent the spatial distribution of seismic strain constituting the field, and the temporal factor $\vec{T}_p$ represents the dynamic characteristics of the strain fields at different times. Due to the symmetry of the matrix, the eigenvalues obtained were positive real numbers, the eigenvalues were arranged from large to small, and the eigenvectors corresponding to t eigenvalues satisfy the accuracy of fitting the total strain field, indicating that the first t spatio-temporal variables of the strain field as the research object represent the spatio-temporal characteristics of the total strain field in the study area (the manuscript is the Longmenshan fault zone and its adjacent areas). The fitting accuracy of the first t eigenvalues was:

$$\eta = \frac{\sum_{p=1}^{t} \lambda_p}{\sum_{p=1}^{n} \lambda_p} \tag{7}$$

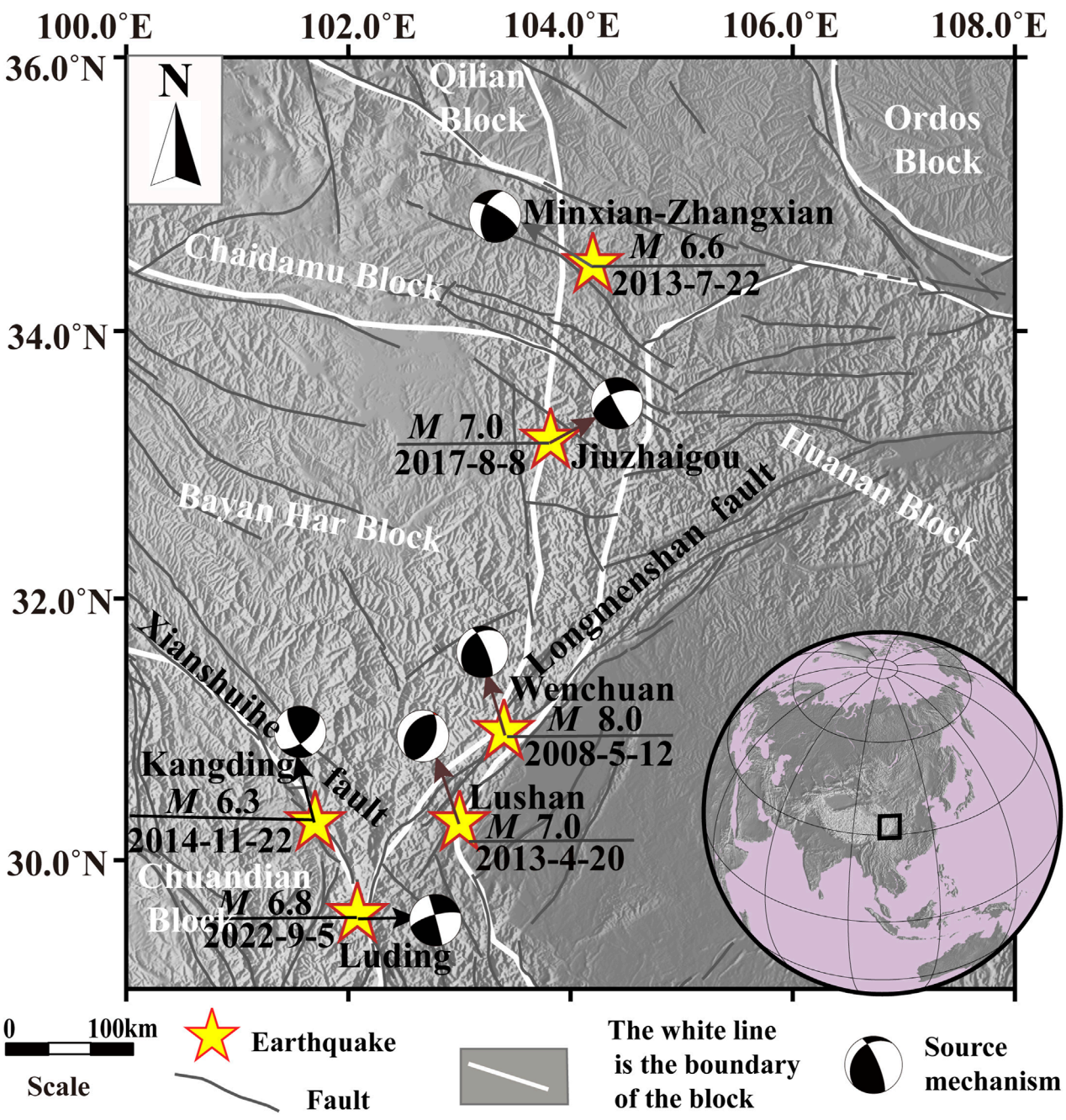

FIGURE 1
Distribution of epicentre and mechanism of $M \geq 6.3$ earthquakes around the Longmenshan fault zone since 2008. Black lines represent fault. The white lines represent the boundary of the block, including the Qilian block, Ordos block, Chaidamu block, Bayan Har block, Chuandain block and Huanan block. The black circle in the lower right corner is the world topographic map. The yellow stars represent the epicentres of six earthquakes of magnitude $M \geq 6.3$, according to data from the China Earthquake Networks Center (CENC). Black source mechanism data from the United States Geological Survey (USGS).

where η (Yang and Ma, 2016) represents the fitting acuracy of the strain field.

The biggest advantage of natural orthogonal function method was that it can extract the main strain fields with anomalies in the study area, which was equivalent to concentrating the main information of the strain fields in the study area in the first t strain fields, focusing on the study of the spatio-temporal anomalies of the first t strain fields, and eliminating the strain fields with no abnormalities or no obvious abnormal changes. The spatiotemporal anomalies of t main strain fields were studied to simplify complex problems.

2.2 Study objects and data sources

This study focused on six strong earthquakes that occurred in the vicinity of LFZ since 2008: the 2008 Wenchuan (M8.0) earthquake, 2013 Lushan (M7.0) earthquake, 2013 Min County–Zhang County (M6.6) earthquake, 2014 Kangding (M6.3) earthquake, 2017 Jiuzhaigou (M7.0) earthquake, and 2022 Luding (M6.8) earthquake (Figure 1). The focal mechanism solution data for these six earthquakes were mainly supplied by the US Geological Survey (USGS), and the earthquake catalog data for the study area were provided by the China Earthquake Networks Center (CENC). Since 1995, the b-values of small and medium earthquakes in the study area have been calculated, and the minimum complete magnitude was determined to be M2.0 (Yang et al., 2017; Luo et al., 2019). Considering that the probability of moderate or stronger earthquakes occurring is generally very low, and the release of seismic strain has a significant impact on the study area, a lower limit of M2.0 and an upper limit of M5.0 were selected for the earthquake magnitude range to ensure that the selected data fully reflected the contextual seismic activity in the region and the development of strong earthquake sources (Table 1). In principle, aftershocks were not deleted; however, for overlapping areas of impact between strong earthquakes, it was necessary to delete the aftershocks of the previous six earthquakes to avoid affecting the subsequent strong earthquake. For example, the study areas of the 2008 Wenchuan (M8.0) earthquake and 2013 Lushan (M7.0) earthquake partially overlapped; therefore, to study the seismic strain field before the Lushan earthquake, it employed the K-K theory (Luo et al., 2019) to delete the aftershocks of the Wenchuan (M8.0) earthquake.

2.3 Spatio-temporal extent of selected data

Two spatial statistical scales were selected for the six earthquakes. The first scale was for seismically active areas related to the strong earthquake hypocenters, referred to as the research area and set to be no less than 3° × 3° (Yang et al., 2017; Luo et al., 2023). The second scale was a smaller statistical unit used for calculating anomalies, known as the grid; its size was set at 0.5° × 0.5°. The rationale for selecting these two spatial regions was as follows. First, the statistical areas of different focal scales are associated with the size of the seismogenic structure. Mei, S. R. (1997) studied the long-term anomaly evolution process before three earthquakes of ≥ M7 in the North China Plain. They estimated the seismically active area to be within 400–500 km and found that it gradually reduced during the evolution process. They stated that the extent of the seismically active area in the 10 years before the earthquake was approximately 3°–4°. Based on this, a range of approximately 3° longitude and latitude around the epicenter of six earthquakes were selected as different study areas, making adjustments considering factors such as earthquake magnitude, the scale of the seismogenic structure, and the distribution of seismic activity. This selected range included both the stages of strengthening and weakening of seismic activity before an earthquake. When calculating the strain field of strong earthquakes, grids with equal intervals are utilized, and the grid size needs to reflect the anomaly characteristics of the regional strain field. If the grid is too dense, the distribution of the strain field will become fragmented, making it difficult to discern the main characteristics. Conversely, if the grid is too sparse, the anomaly characteristics of seismic activity will not be well reflected, leading to weakened anomaly differences and the loss of important anomaly information. Therefore, based on previous research (Luo et al., 2023), a grid unit of 0.5° × 0.5° was selected.

2.4 Computation procedure

The procedure for calculating the seismic strain field was as follows. Firstly, the area was divided into grid units of 0.5° × 0.5°. A time interval of a year and a sliding step of a month were used, ensuring that there was a minimum of 10 years' worth of seismic data in the area. Secondly, the seismic strain field matrix $\boldsymbol{S}$ was constructed, and the covariance matrix $\boldsymbol{R}$ was solved to obtain the eigenvalues of the main strain field. Finally, using the aforementioned research method, the temporal factor and contours of the main strain field corresponding to the eigenvalues were calculated to analyze the relationships between anomalies and strong earthquakes.

3 Results

3.1 Strain field temporal factor variation

In this study, the natural orthogonal function was used to calculate the strain field of the six strong earthquakes in the vicinity of LFZ that have occurred since 2008. When t is equal to 4, the first 4 strain fields have exceeded 80% of the total strain field. Before the 2013 Lushan (M7.0) earthquake, the strain field exceeded 92%, indicating that the anomaly information of the regional strain fields before these six strong earthquakes was concentrated in the first 4 main strain fields.

Table 2 shows the seismic strain field temporal factor before the six strong earthquakes, including calculation grids and time interval, time of anomaly for the first 4 strain field temporal factors, type of anomaly, mean-square-error, and accuracy as a proportion of the total fields. When the strain field temporal factor exceeded the mean square error before a strong earthquake, it was considered an anomaly (Luo et al., 2023). Anomalies were divided into long-term (2–10 years before the earthquake), medium-term (from 3 months to 2 years before the earthquake), short-term (1–3 months before the earthquake), and impending (several days before the earthquake).

Figure 2 shows the temporal factors of the seismic strain before the six strong earthquakes in the vicinity of LFZ. The results show whether the increase or decrease in the temporal factors of the strain fields exceeded the mean square error. Before the 2008 Wenchuan (M8.0) earthquake, 2013 Lushan (M7.0) earthquake, and 2022 Luding (M6.8) earthquake, the regional strain field showed obvious short-term anomalies. Impending-earthquake anomalies appeared in the main strain field (T3) of the Wenchuan (M8.0) earthquake and the main strain field (T1) of the Lushan (M7.0) earthquake (Table 2). In 2013, before the Zhang County–Min County (M6.6) earthquake, there were medium-term anomalies in the strain field. Except for T4, the other three strain field anomalies were affected by the relatively large strain field anomaly of the Wenchuan (M8.0)

TABLE 1 Seismic data of six strong earthquakes around the Longmenshan fault zone since 2008.

No.	Earthquake	Coordinates of the study area [lat. (º) and long. (º)]	Time span of the data	Focal mechanism solution nodal section I (º)			Focal mechanism solution nodal section II (º)			Data source
				Strike	dip	rake	Strike	dip	rake	
1	2008-05-12 Wenchuan (Sichuan), M_s 8.0	30.0°–33.5° 101.5°–106°	1995-01–2008-04	222	29	152	336	79	63	USGS
2	2013-04-20 Lushan (Sichuan), M_s 7.0	29.5°–31.5° 102.5°–105.5°	2000-01–2013-03	218	39	103	21	52	79	USGS
3	2013-07-22 Minxian-Zhangxian (Gansu),M_s 6.6	33.0°–36.5° 103.0°–106.5°	2000-01–2013-06	302	73	41	197	51	157	USGS
4	2014-11-22 Kangding (Sichuan), M_s 6.3	28.5°–32.0° 100.5°–103.0°	2000-01–2014-10	151	70	33	48	59	156	USGS
5	2017-08-08 Jiiuzhaigou (Sichuan), M_s 7.0	32.0°–34.5° 102.5°–105.0°	2000–01–2017–07	246	57	−173	152	84	−33	USGS
6	2022-09-05 Luding (Sichuan), M_s 6.8	28.0°–31.0° 100.5°–103.5°	2014-01–2022-08	345	88	17	254	73	177	USGS

Note: The time of the earthquake is Beijing time, and the earthquake directory is from China Earthquake Networks Center. Additional data for columns 5 through 10 are primarily from the United States Geological Survey.

10.3389/feart.2024.1269753

10.3389/feart.2024.1269753

TABLE 2 Parameters of the strain field temporal factors of 6 *Ms* ≥6.3 earthquakes around the Longmenshan fault zone since 2008.

No.	Earthquake	Grids (n, m)	Anomaly centroid (°N, °E)	Temp-oral factor	Time of anomaly (year-month)	Mean square error	Type of anomaly	Accura-cy *r*
1	2008-05-12 Wenchuan Ms 8.0	(63,158)	32.3,101.7	T1	2006-05–11	±2.0	Medium term	0.86
			33.0,104.7	T2	2005-07–12	±1.2	Long-to-medium term	
			30.2,103.2	T3	2008-02–04	±1.0	Short-to-imminent term	
				T4	2007-04–06	±0.8	Medium term	
2	2013-04-20 Lushan Ms 7.0	(24,157)	30.5,102.5 31.5,103.6 29.5,105.5	T1	2013-02–03	±1.4	Short-to-imminent term	0.92
				T2	2012-01–03	±1.3	Medium term	
				T3	2012-10–12	±0.5	Medium term	
				T4	2012-02–09	±0.4	Medium term	
3	2013-07-22 Minxian-Zhangxian Ms 6.6	(49,160)	34.5,104.3	T1	2003-08–10	±2.5	Long term	0.86
				T2	2006-08–09[a]	±2.1	Long term	
				T3	2005-04–06[a]	±1.1	Long term	
				T4	2011-10–12	±0.8	Medium term	
4	2014-11-22 Kangding Ms 6.3	(35,176)	30.5,102.5 29.8,101.5	T1	2008-02–05[a] 2011-03-05	±1.0	Long term	0.83
				T2	2008-02–05[a] 2011-03-05	±1.0	Long term	
				T3	2003-10–12 2008-02–05[a]	±0.7	Long term	
				T4	2008-05–07[a]	±0.7	Long term	
5	2017-08-08 Jiiuzhaigou Ms 7.0	(16,209)	32.5,104.6 34.2,102.2	T1	2006-04–06	±1.8	Long term	0.80
				T2	2008-03–05[a]	±1.4	Long term	
				T3	2005-05–2006-04	±0.9	Long term	
				T4	2013-05–11	±0.7	Long term	
6	2022-09-05 Luding Ms 6.8	(36,102)	28.5,103.5 29.6,102.2	T1	2014-11–2015-03	±2.6	Long term	0.88
				T_2	2018-03–07 2022-04-07	±2.4	Long and short term	
				T_3	2018-03–07 2022-03–07	±2.2	Long and short term	
				T_4	2021-05–09 2022-06-08	±1.8	Medium and short term	

Note: n, number of grids; m, time interval. T_k is the *k*th (1–4) strain-field time factor.

[a]Indicates that the period was affected by the *M*s 8.0 wenchuan earthquake.

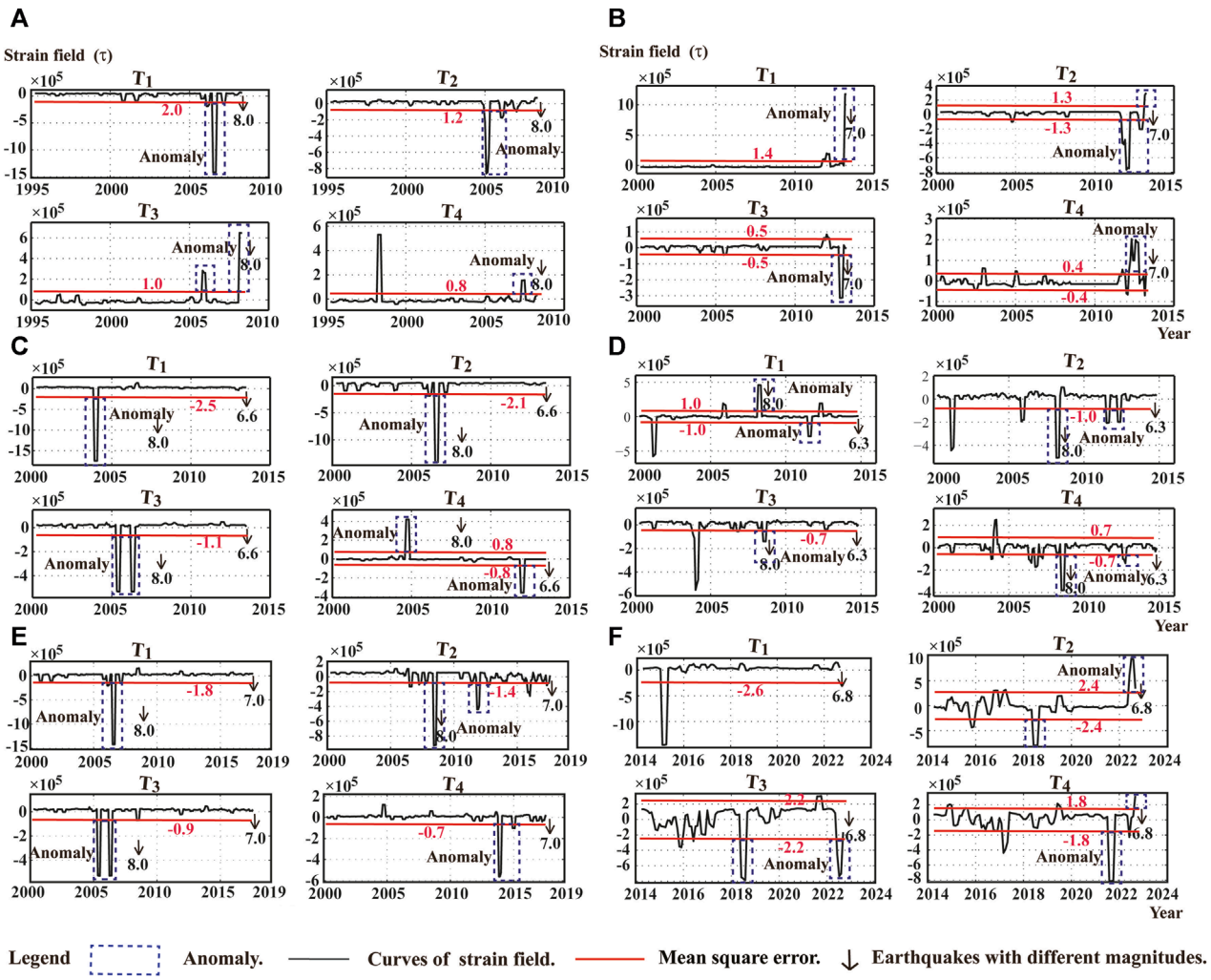

FIGURE 2
Temporal factors of the first 4 strain fields of 6 $M \geq 6.3$ earthquakes around the Longmenshan fault zone since 2008. The green dotted line represents the anomaly, the red line is the mean square error, the black arrow represents the magnitude of a $M \geq 6.3$ earthquake. **(A)** 2008 Wenchuan (*M*8.0) earthquake; **(B)** 2013 Lushan (*M*7.0) earthquake; **(C)** 2013 Minxian-Zhangxian (*M*6.6) earthquake; **(D)** 2014 Kangding (*M*6.3) earthquake; **(E)** 2017 Jiuzhaigou (*M*7.0) earthquake; **(F)** 2022 Luding (*M*6.8) earthquake.

earthquake. There were no short-term anomalies in the strain field before the 2014 Kangding (*M*6.3) earthquake or 2017 Jiuzhaigou (*M*7.0) earthquake. Medium-term anomalies were also affected by the Wenchuan (*M*8.0) earthquake.

3.2 Interactions between strong earthquakes in the southern LFZ

According to Table 1, the study area of the 2008 Wenchuan (*M*8.0) earthquake was 30°–33.5°N and 101.5°–106.0°E; that of the 2013 Lushan (*M*7.0) earthquake was 29.5°–31.5°N N and 101.5°–106.0°E. These two study areas partially overlapped, but their temporal factor anomaly curves were different. Therefore, it was necessary to compare the differences in the strain field temporal factors between the two, and to determine whether there was any mutual influence between the earthquakes. A study area was selected to include both earthquakes (29.5°–33.5°N, 101.5°–106.5°E). The area of a strain field with a contour value (or absolute value) greater than 0.05×10^5 before a strong earthquake is considered to be an anomaly area (Luo, et al., 2019). Positive contours represent released strain and negative contours represent accumulated strain. Points where positive and negative contours intersect along large active faults are often the locations of future strong earthquakes (Luo, et al., 2023).

Figure 3A shows the strain field contour distribution before the 2008 Wenchuan (*M*8.0) earthquake (1 January 2000, to 11 May 2008). The anomaly areas were concentrated at 31.7°–32.7°N & 101.5°–102.3°E and 32.7°–33.5°N & 104.3°–105.3°E. These two areas were outside of the study area forthe Lushan (*M*7.0) earthquake, confirming that the four strain field temporal factor anomalies before the Lushan earthquake were not affected by the Wenchuan (*M*8.0) earthquake. The LFZ did not have notable contour anomalies, but the Wenchuan (*M*8.0) earthquake still

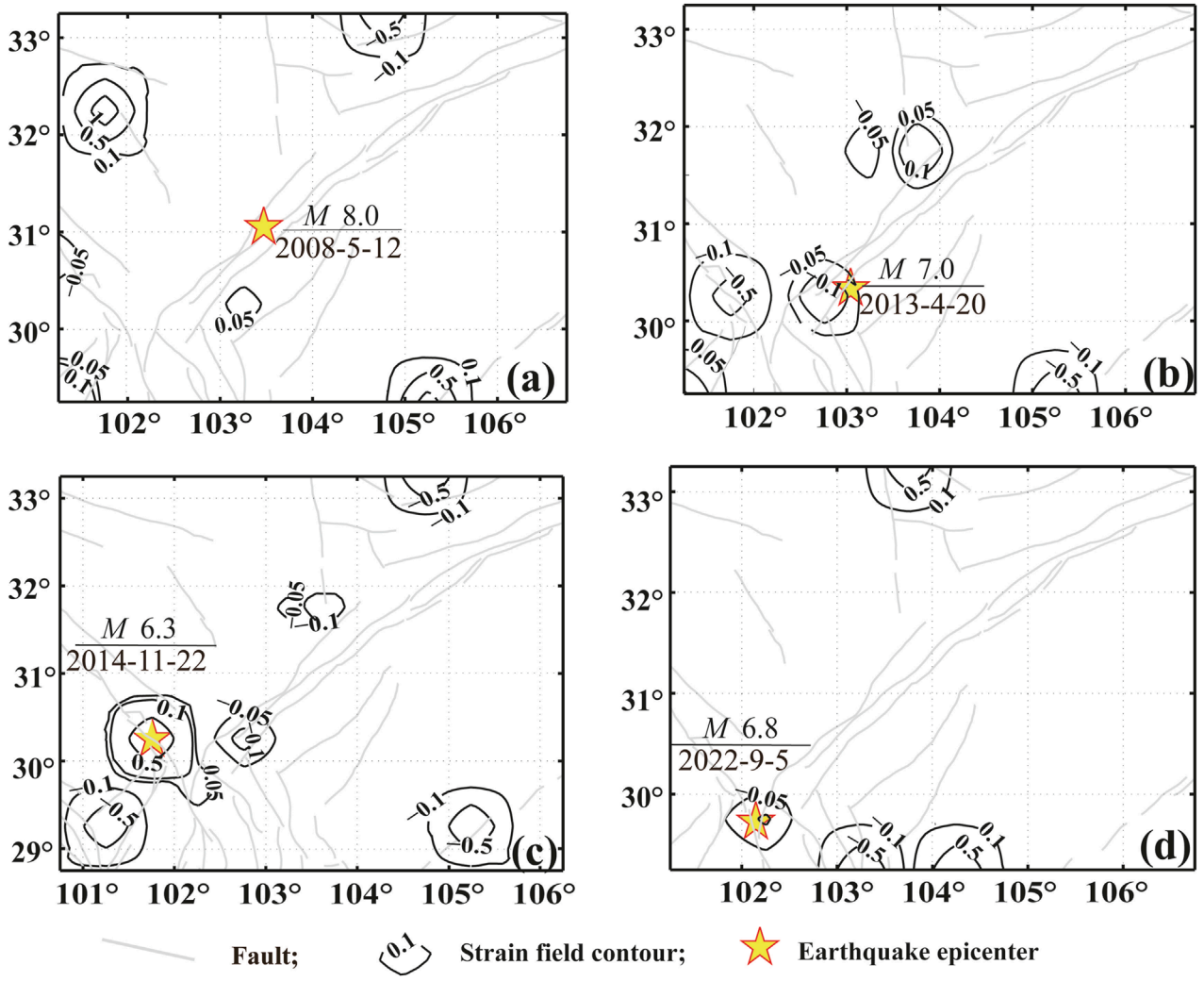

FIGURE 3
Spatial isoline distribution of strain field before Wenchuan, Lushan, Kangding and Luding earthquakes. The gray line is the fault, the black line is the strain field contour line, negative value represents the accumulated strain and the positive value represents the released strain, the isoline value 0.1 represents 0.1 times 10^5. The yellow stars represents the epicenter of strong earthquake. **(A)** Strain field from 1 January 2000 to 11 May 2008; **(B)** Strain field from 1 January 2009 to 19 April 2013; **(C)** Strain field from 1 January 2009 to 21 November 2014; **(D)** Strain field from 1 January 2015 to 4 September 2022.

occurred. Figure 3B shows the evolution of the strain field contours before the 2013 Lushan (*M*7.0) earthquake (1 January 2009, to 19 April 2013). The anomaly areas were concentrated at 29.5°–30.7°N & 101.5°–103.3°E and 31.5°–32.2°N & 103.3°–104.3°E. The 2013 Lushan (*M*7.0) earthquake occurred on the edge of the former anomaly area. Figure 3C shows the anomaly areas of the strain field spatial equivalent before the 2014 Kangding (*M*6.3) earthquake (1 January 2009, to 21 November 2014). After the Wenchuan (*M*8.0) and Lushan (*M*7.0) earthquakes, the area of strain field anomalies in the vicinity of where the Xianshuihe Fault Zone intersects with the LFZ increased, and the 2014 Kangding (*M*6.3) earthquake occurred in the high-value anomaly area. Figure 3D shows the contours of the strain field before the 2022 Luding (*M*6.8) earthquake (1 December 2014, to 4 September 2022). The anomaly areas are mainly concentrated at 29.5°–30.0°N and 102.0°–104.5°E. The Luding (*M*6.8) earthquake occurred on the edge of the anomaly area. These results indicate that since 2009, the southern section of LFZ, where it intersects with the Xianshuihe Fault Zone, has experienced high-value anomalies. The 2013 Lushan (*M*7.0) earthquake, 2014 Kangding (*M*6.3) earthquake, and 2022 Luding (*M*6.8) earthquake all occurred in this vicinity and were all affected by the 2008 Wenchuan (*M*8.0) earthquake.

3.3 Interactions among strong earthquakes in the northern LFZ

As shown in Table 1, the study areas of the Wenchuan, Min-Zhang, and Jiuzhaigou earthquakes are different, but with small overlaps. A study area containing all three strong earthquakes (30.0°–36.5°N, 101.5°–106.5°E) was chosen to analyze the spatial evolution of seismic strain field anomalies.

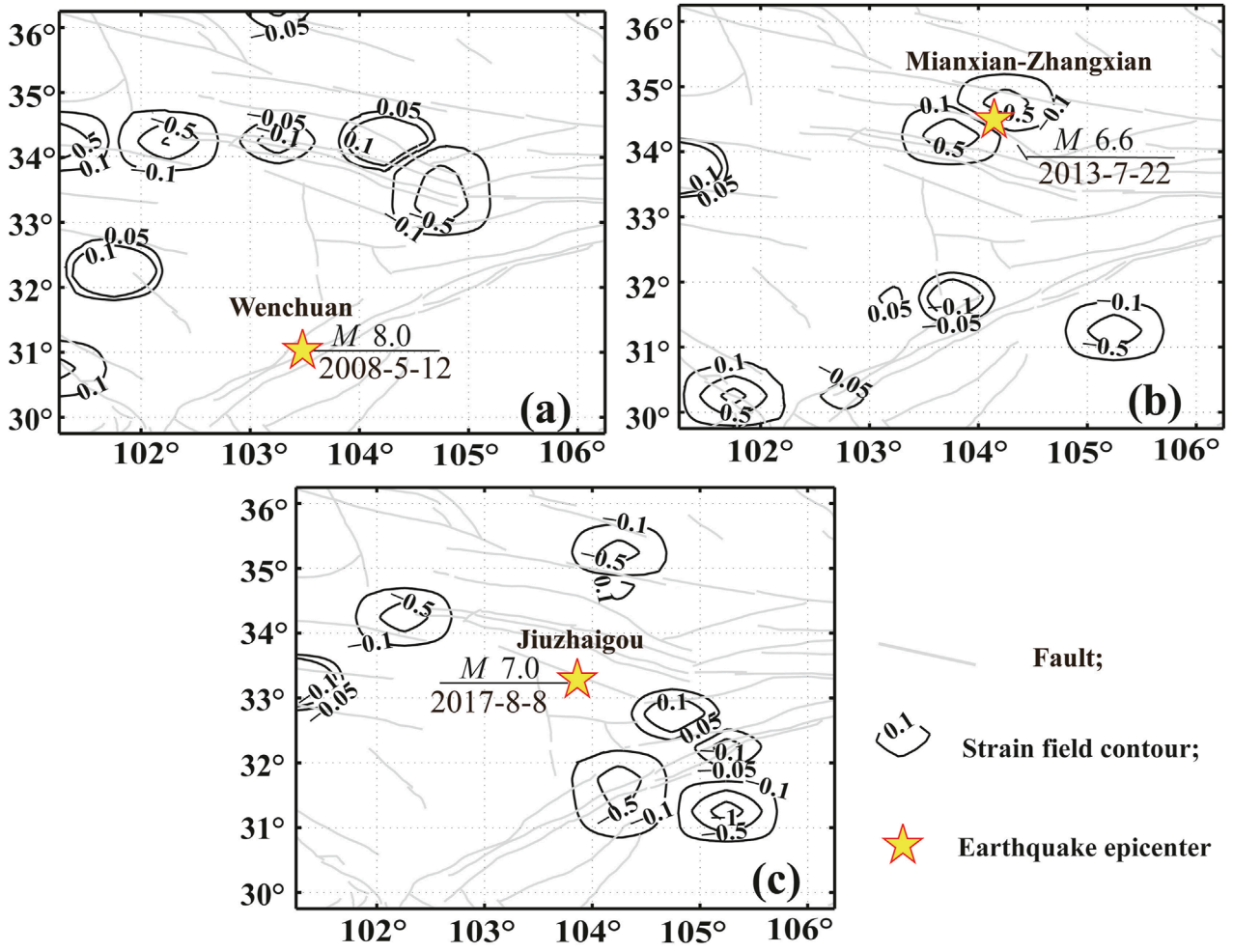

FIGURE 4
Spatial isoline distribution of strain field before Wenchuan, Minxian-Zhangxian and Jiuzhaigou earthquakes. The gray line is the fault, the black line is the strain field contour line, negative value represents the accumulated strain and the positive value represents the released strain, the isoline value 0.1 represents 0.1 times 10^5. The yellow stars represents the epicenter of strong earthquake. **(A)** Strain field from 1 January 2000 to 11 May 2008; **(B)** Strain field from 1 January 2009 to 2 July 2013; **(C)** Strain field from 22 July 2013 to August 2017.

Figure 4A shows that in the period before the 2008 Wenchuan (*M*8.0) earthquake (1 January 2000, to 11 May 2008); seismic strain field contour anomalies were mainly concentrated in the eastern Kunlun Fault, with anomalies distributed in patches around the 34° north line. Special anomalies were concentrated at 33.0°–34.7°N and 103.8°–105.3°E, in the vicinity of the epicenters of the 2013 Min County–Zhang County (*M*6.6) and 2017 Jiuzhaigou (*M*7.0) earthquakes, indicating that anomalies formed decades before these strong earthquakes. There were no anomalies in the epicentral area of the Wenchuan (*M*8.0) earthquake, which is consistent with the results in Figure 4A.

Figure 4B were the contour distribution of the strain field in the period before the 2013 Min County–Zhang County (*M*6.6) earthquake (1 January 2009, to 21 July 2013). It shows that the strain field anomalies after the Wenchuan earthquake were mainly concentrated in the area of 33.8°–35.2°N and 103.3°–104.7°E, except for LFZ. This area is also in the vicinity of the epicenters of 2013 Min County–Zhang County (*M*6.6) and 2017 Jiuzhaigou (*M*7.0) earthquakes. Before the Wenchuan earthquake, an anomaly area formed in this region. After the Wenchuan earthquake, anomalies increased significantly in this area. The more northerly location of the anomalies further indicated that the Wenchuan earthquake had a certain influence on the Min County–Zhang County and Jiuzhaigou earthquakes. Figure 4C shows the strain field contours before the 2017 Jiuzhaigou (*M*7.0) earthquake (22 July 2013, to 7 August 2017). After the 2013 Min County–Zhang County (*M*6.6) earthquake, regional strain field anomalies were mainly distributed in the northern central parts of LFZ and could have been related to the 2017 Jiuzhaigou (*M*7.0) earthquake. Comparing Figures 4A–C, the Wenchuan and Jiuzhaigou earthquakes were found to occur at the center of a ring of anomalies in the seismic strain field, with no anomalies in the vicinity of the epicenters, while the Min County–Zhang County earthquake occurred in the strain field anomaly area.

In summary, by studying the spatio-temporal evolution of the strain fields of six earthquakes in the vicinity of LFZ, the seismic

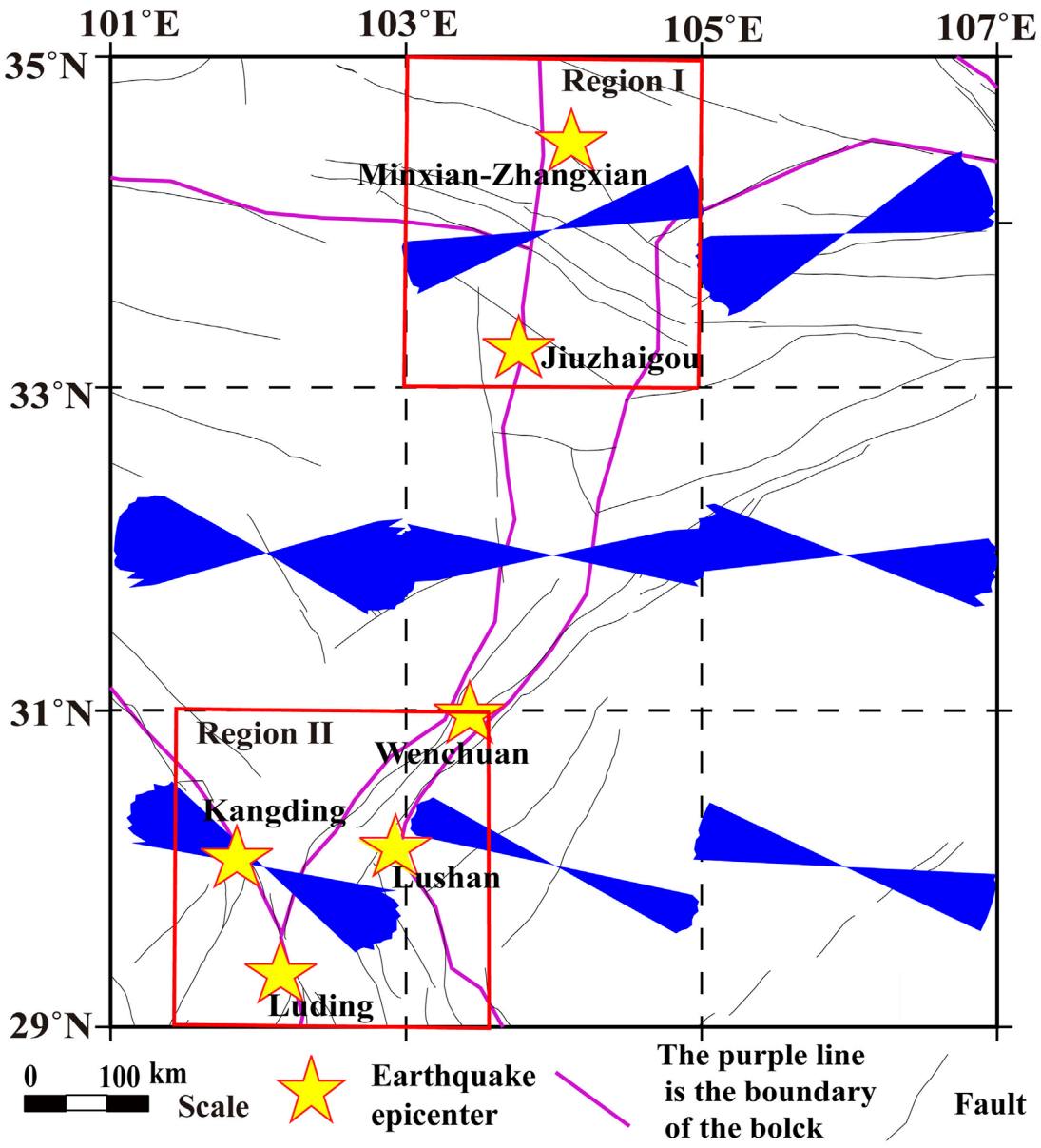

FIGURE 5
Zoning results of seismic tectonic stress field around the Longmenshan fault zone (Wang et al., 2015). The blue rose leaves represent the direction of the principal compressive stress in the 2° × 2° region. The red line frame represents the study area, where regionIcontains the Minxian-Zhangxian *M*6.6 earthquake and the Jiugouzhai (*M*7.0) earthquake, and region II contains the Wenchuan (*M*8.0) earthquake, Lushan (*M*7.0) earthquake, Kangding (*M*6.3) earthquake and Luding (*M*6.8) earthquake. The yellow stars represent the epicenters of six earthquakes. Black lines show major faults. The purple lines represent the boundary of the block.

strain field temporal factor anomalies were found to be closely related to contour anomalies. Controlled by regional tectonics and stress fields, seismic strain in fault zones is accumulated or released, resulting in changes in seismic strain field anomalies over time. The southern region of LFZ intersects with the Xianshuihe Fault Zone. The development and occurrence of the 2008 *M*8.0 Wenchuan and 2013 Lushan (*M*7.0) earthquakes inevitably restrained the Xianshuihe Fault Zone. This also explains the 2014 *M*6.3 Kangding and 2022 Luding (*M*6.8) earthquakes. The northern section of LFZ intersects with the Minjiang Fault, Huya Fault, and Wenxian Fault. The development of strong earthquakes on these faults will inevitably be mutually restraining and regulating, which explains the mutual influences of the 2008 Wenchuan (*M*8.0) earthquake, 2013 Min County–Zhang County (*M*6.6) earthquake, and 2017 Jiuzhaigou (*M*7.0) earthquake. This result is consistent with the *b*-value method (Yi et al., 2013; Liu and Pei, 2017) and Benioff strain method (Li et al., 2022) study the influence of stress and strain changes on strong earthquakes

10.3389/feart.2024.1269753

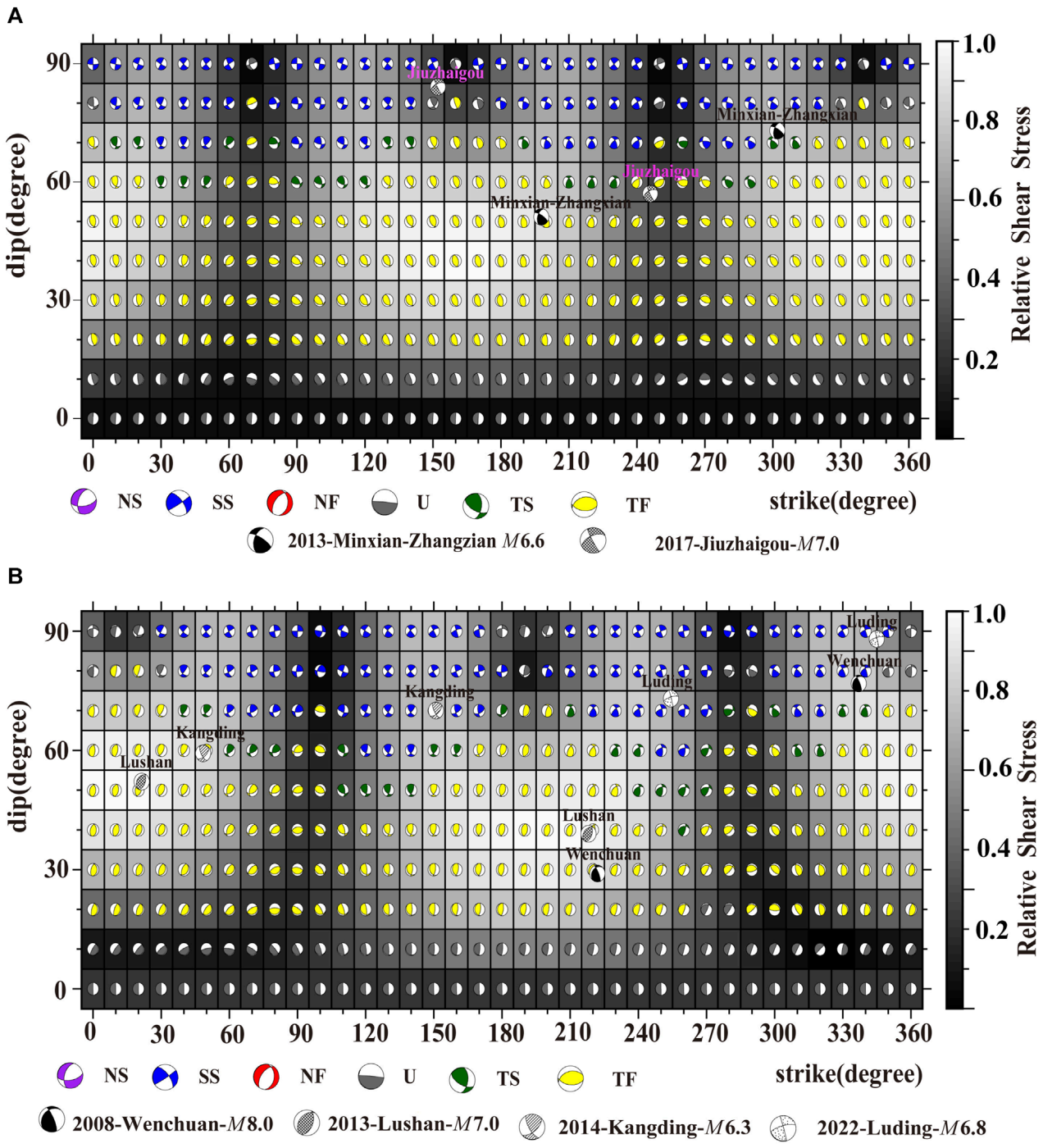

FIGURE 6
The shear stress result of the tectonic stress field around Longmen Mountain fault at the focal plane of strong earthquake. The abscissa is the strike of the focal mechanism, and the ordinate is the dip Angle. With 10° as the step length for both horizontal and vertical coordinates, theoretical numerical simulation focal mechanism solutions of different node surface shapes were divided. NS represented positive fault-and-strike slip type, SS represented strike slip type, NF represented positive fault-and-strike slip type, TS represented reverse fault-and-strike slip type, TF represented reverse fault-and-strike type, and U represented uncertain focal mechanism solutions. The background colors of the grid squares from black, grey to white represent the shear stress from small to large under the stress system. **(A)** The focal mechanism joint shear stress results in region I are compared with the USGS focal mechanism solutions for the Minxian-Zhangxian earthquake and the Jiuzhaigou earthquake. **(B)** The nodal shear stress results of the theoretical focal mechanism solution for region II are compared with those of the USGS Wenchuan, Lushan, Kangding and Luding earthquakes.

in the LFZ. Strong earthquakes occur around low *b* value and high stress, after strong earthquakes, the *b* value of the region recovers obviously and gradually increases. On the Benioff strain curve, the cumulative strain in the region rises obviously and the slope of the curve becomes larger within 1 year after the earthquake.

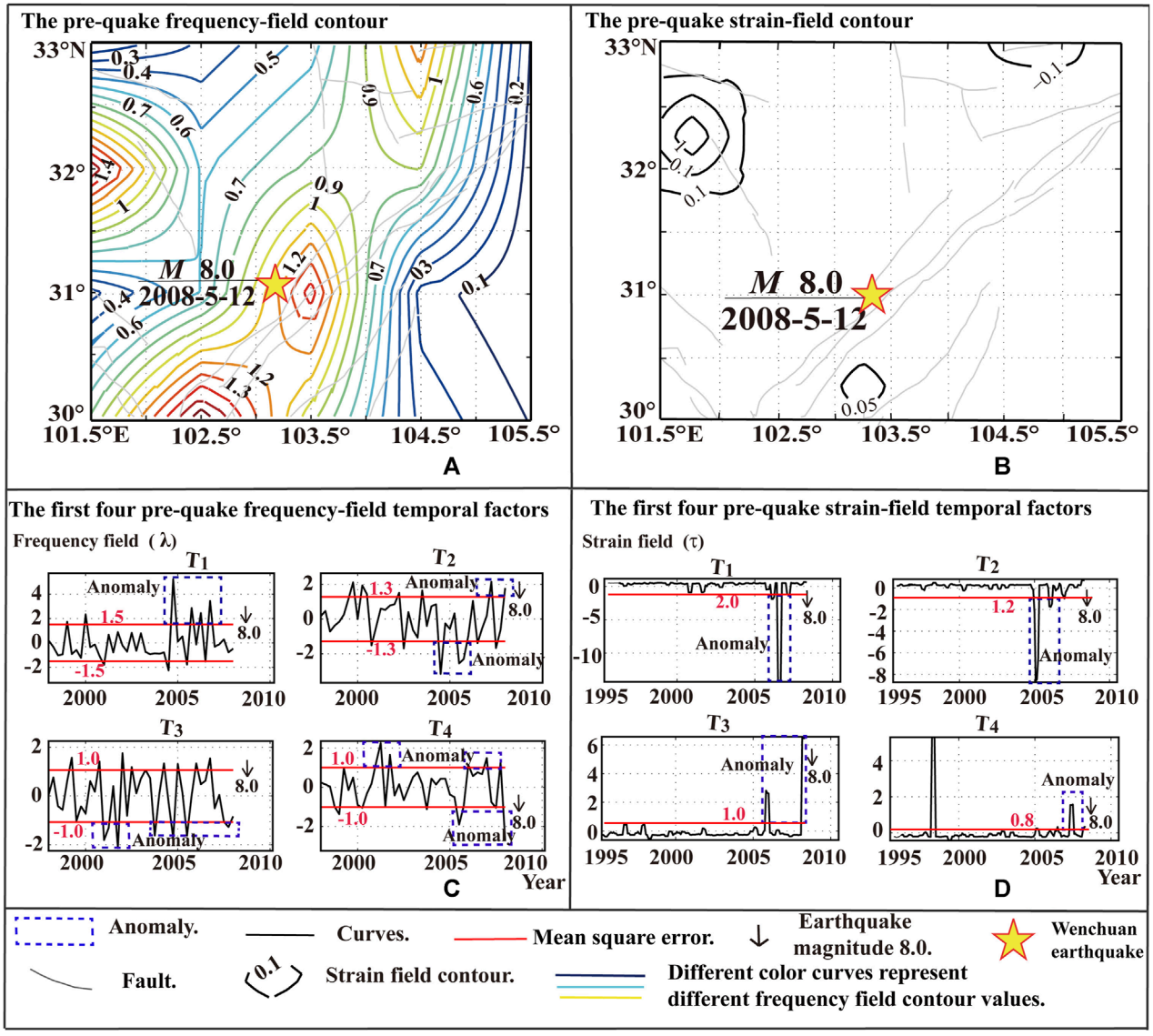

FIGURE 7
Temporal and spatial anomalies of frequency field and strain field before the 2008 Wenchuan (*M*8.0) earthquake. The pre-quake frequency-field of spatial contour anomalies distribution **(A)**; The pre-quake strain-field of spatial contour anomalies distribution **(B)**; The first 4 pre-quake frequency-field of temporal factors anomalies distribution **(C)**; The first 4 pre-quake strain-field of temporal factors anomalies distribution **(D)**.

3.4 Comparison of NOF results with shear stress results of focal mechanism node

Based on previous research reports (Wang et al., 2015) on the zoning of the tectonic stress system in the vicinity of LFZ (Figure 5), the principal compressive stress direction in region I was northeastern, and the stress field parameters were compressive axis strike of 72°, inclination angle of 2°, long-axis strike of 304°, plunge of 87°, and stress shape factor R-value of 0.68. The principal compressive stress direction of region II was northwesterly, and the stress field parameters were a final axis strike of 103°, inclination angle of 8°, long-axis strike of 226°, plunge of 82°, and stress shape factor R-value of 0.76. Based on the stress field parameters of the two regions, and using focal mechanism and shear stress Method in Regional tectonic Stress Field (Wan, 2020), the relative shear stress of the two nodal planes of the focal mechanism solutions (from the USGS) of the 2013 Min County–Zhang County (*M*6.6) earthquake and 2017 Jiuzhaigou (*M*7.0) earthquake in region I were calculated (Figure 6A). The results show that the relative shear stress of the Min County–Zhang County earthquake was large, and the seismic stress was fully released; whereas, that of the Jiuzhaigou earthquake was small, and the seismic stress was not fully released. The relative shear stress of the two nodal planes of the focal mechanism solutions (from USGS) of the 2008 Wenchuan (*M*8.0) earthquake, 2013 Lushan (*M*7.0) earthquake, 2014 Kangding (M6.3) earthquake, and 2022 Luding (*M*6.8) earthquake in region II were calculated (Figure 6B). The results show that the relative shear stress of the Wenchuan and Lushan earthquakes were larger, and the seismic stress was fully released; as such, the risk of powerful earthquakes in LFZ was low. However, the relative shear stresses of the Kangding

TABLE 3 Temporal and spatial anomalies of strain field and frequency field before the 2008 Wenchuan *Ms* 8.0 earthquake.

Earthquake	Seismic field	Temporal factor anomaly			Spatial contour anomaly		
		Time of anomaly (ear-month)	Temporal factor	Type of anomaly	Anomaly centroid [° N, °E)]	Anomaly radiu (km)	Distance between anomaly center and earthquake (km)
2008–05-12 Wenchuan M_s 8.0	Frequency field	2004-07–12	T_1, T_2	Long-to-med-ium term	32.1,101.5	56	210
		2005-07–12	T_2, T_3	Long-to-med-ium term	33.0,104.5	42	245
		2006-10–12	T_1	Medium term	30.0,102.5	34	140
		2008-01–04	T_4	Short-to-Immin-ent term	31.0,103.6	26	0
	Strain field	2005-07–12	T_2, T_3	Long-to-med-ium term	32.3,101.7	39	213
		2006-05–11	T_1	Medium term	33.0,104.7	27	252
		2007-04–06	T_4	Medium term	30.2,103.2	21	100
		2008-01–04	T_3	Short-to-immi-nent term			

Note: T_k is the *k*th (1–4) strain-field time factor.

and Luding earthquakes were smaller, and the seismic stress was not fully released, resulting in an elevated risk of future events; 7 years after the Kangding (*M*6.3) earthquake, the 2022 Luding (*M*6.8) earthquake occurred ~85 km away.

In the vicinity of LFZ, the results of strain field obtained by natural orthogonal function (EOF) method are basically consistent with the results of shear stress generated by regional tectonic stress field at focal mechanism node. The 2008 Wenchuan (*M*8.0) earthquake and 2013 Lushan (*M*7.0) earthquake had larger shear stresses, and the seismic stress was fully released, which had significant impacts on surrounding tectonic fault stress. There were also notable medium-term and short-term temporal factor anomalies in the strain fields, and the contour anomaly areas were relatively large. Conversely, theKangding (*M*6.3) earthquake, Jiuzhaigou (*M*7.0) earthquake, and Luding (*M*6.8) earthquake had relatively smaller shear stresses, and the seismic stress was not fully released, creating a small impact on the surrounding tectonic fault stress. There were few short-term temporal factor anomalies, and the contour anomaly areas were relatively small.

4 Discussion

4.1 Spatio-temporal anomalies of strain and frequency fields

The results of this study were compared with previous research on the frequency field of LFZ (Luo et al., 2023) to identify differences in spatial and temporal anomalies of the frequency and strain fields. Taking the 2008 Wenchuan (*M*8.0) earthquake as an example (Figure 7), the time intervals of the first 4 temporal factor anomalies were the same between the studies. The distribution of the temporal factors (i.e., which temporal factor the anomalies are distributed in) was the key difference. The central area of contour anomalies was largely similar, but the number of anomalies differs (Table 3). Before the 2008 Wenchuan (*M*8.0) earthquake, there were four central areas of high-value frequency field contour anomalies (Luo et al., 2023) and three centers of strain field contour anomalies. These three anomaly locations were all approximately the same distance from the center of the Wenchuan earthquake. The difference is that there was an anomaly area in the frequency field in the vicinity of the Wenchuan epicenter, but not in the strain field. In summary, a comparison of the spatial anomalies of the frequency and strain fields showed that they were largely consistent. However, temporal factor anomalies were easily identifiable in the strain field, and contour anomaly information was more comprehensive in the frequency field.

4.2 Reasons for anomalies

By comparing the frequency and strain fields (Figure 7), and searching the seismic catalog in the study area, the factors affecting spatio-temporal anomalies in the two fields were discovered to be different. Frequency field temporal factor changes fluctuated considerably, and anomalies were complex. The contour anomalies mainly had high gradients and dense distributions. This may be because the spatial and temporal anomalies in the frequency field

were primarily affected by the occurrence of minor earthquakes in the region. Nevertheless, changes in the temporal factors of the strain fields were relatively systematic, with prominent anomalies. High-value strain field spatial and temporal anomalies were relatively sporadic. This may be because spatial and temporal anomalies in the strain field were primarily affected by moderate earthquakes. In summary, in this region, the frequency field was primarily affected by the frequency of *M*2–3 earthquakes, and the strain field was mainly affected by *M*4–5 foreshocks.

4.3 Orthogonal function as a forecasting tool

The identification of earthquake precursors is of great significance to earthquake forecasting. This study used the orthogonal function, which is commonly used in atmospheric and climate science (Lorenz, 1956; Obukhov, 1960), to identify strong earthquake precursors in the vicinity of LFZ for earthquake forecasting. Earthquake forecasting remains a contentious scientific issue. However, recently, significant progress is seen in medium-term and short-term seismicity-based forecasting techniques. The approaches can be divided into 7 physical process-based models and 10 smoothed seismicity-based models (Tiampo and Shcherbakov, 2012). The natural orthogonal function becomes 11 techniques to use the smoothed seismicity-based model. More earthquake forecasting information is provided in the spatially and temporally of strain field, but it is limited by the relatively short time of earthquake catalogs data. In order to evaluate the application of orthogonal function in earthquake prediction, it is necessary to accumulate seismic observation data over a long period.

5 Conclusion

In this study, the spatio-temporal anomalies of seismic strain fields were investigated before and after six strong earthquakes that have occurred since 2008 in the LFZ. Temporal factor anomalies were mainly concentrated in the first 4 strain fields. All the first 4 strain fields had medium- and long-term anomalies that was over the mean square error, and some temporal factors had short-term anomalies (For example, the Wenchuan *M*8.0 and Lushan *M*7.0 earthquakes). More anomaly components produced more reliable results. Areas at intersections of strain accumulation and strain release, or central areas surrounded by multiple high-value strain field anomalies, are often places where powerful earthquakes subsequently occur. The high value anomaly of strain contour is basically consistent with the high value of shear stress of regional tectonic stress field at the focal mechanism plane, which indicates that the orthogonal function method is more reliable in identifying anomalies before strong earthquakes.

Temporal factor anomalies in the strain fields appeared around 2008, and the strong earthquakes occurred several years later in the anomaly area of strain field contours. This indicates that the spatio-temporal anomalies in seismic strain fields of some strong earthquakes in the vicinity of LFZ were affected by the 2008 Wenchuan (*M*8.0) earthquake. Future research should analyze the impact of interactions in strain fields between powerful earthquakes.

Data availability statement

The datasets presented in this study can be found in online repositories. The names of the repository/repositories and accession number(s) can be found in the article/Supplementary material.

Author contributions

GL: Writing–original draft, Formal Analysis, Funding acquisition, Methodology, Software. YX: Conceptualization, Writing–original draft. HL: Data curation, Writing–original draft. FD: Data curation, Writing–original draft. WL: Methodology, Writing–original draft.

Funding

The author(s) declare financial support was received for the research, authorship, and/or publication of this article. This work has been supported by the Ningxia Natural Science Foundation Project (Grant number 2021AAC03483; 2022AAC03687, and 2022AAC03695).

Acknowledgments

Seismic data used in this study were obtained from the Sichuan Earthquake Administration and the China Earthquake Networks Center (CENC). The focal mechanism solution data for these six earthquakes mainly came from the US Geological Survey (USGS).

Conflict of interest

The authors declare that the research was conducted in the absence of any commercial or financial relationships that could be construed as a potential conflict of interest.

Publisher's note

References

Burchfiel, B. C., Royden, L. H., Hilst, R. D. V. D., Hanger, B. H., Chen, Z., King, R. W., et al. (2008). A geological and geophysical context for the Wenchuan earthquake of 12 May 2008, Sichuan, *People's Republic of China*. *GSA Today* 18 (7), 4–11. doi:10.1130/GSATG18A.1

Chen, C. Y., Ren, J. W., Meng, G. J., Yang, P. X., and Su, J. F. (2013). Division, deformation and tectonic implication of active blocks in the eastern segment of Bayan Har block. *Chin. J. Geophys.* 56 (12), 4125–4141. doi:10.6038/cjg20131217

Chen, G. G., Ji, F. J., Zhou, R. J., Xu, J., and Ye, Y. Q. (2007). Primary research of activity segmentation of Longmenshan fault zone since Late-Quaternary. *Seismol. Geol. (in Chinese)* 29 (3), 657–673. doi:10.1016/S1872-5791(07)6004-X

Chen, L. C., Ran, Y. K., Wang, H., Li, Y. B., and Ma, X. Q. (2013). The Lushan *M*s7.0 earthquake and activity of the southern segment of the Longmenshan fault zone. *Chin. Sci.Bull.* 58 (28-29), 3475–3482. doi:10.1007/s11434-013-6009-6

Cheng, J., Yao, S. H., Liu, J., Yao, Q., Gong, H. L., and Long, H. Y. (2018). Visoelastic coulomb stress of historical earthquake on the 2017 Jiuzhaigou earthquake and the subsequent influence on the seismic hazards of adjacent faults. *Chinese J. Geophys. (in Chinese)* 61 (5), 2133–2151. doi:10.6038/cjg2018L0609

Clark, M. K., and Royden, L. H. (2000). Topographic ooze: building the eastern margin of Tibet by lower crustal flow. *Geology* 28 (8), 703–706. doi:10.1130/0091-7613(2000)028<0703:tobtem>2.3.co;2

Deng, Q. D., Chen, S. F., and Zhao, X. L. (1994). Tectonics, seismicity and dynamics of longmenshan mountains and its adjacent regions. *seismology and Geology* 16 (4), 389–403. (in Chinese).

Diao, F. Q., Wang, R. J., Wang, Y. B., Xiong, X., and Walter, T. R. (2018). Fault behavior and lower crustal rheology inferred from the first seven years of postseismic GPS data after the 2008 Wenchuan earthquake. *Earth and Planetary Science Letters* 495, 202–212. doi:10.1016/j.epsl.2018.05.020

Du, F., Long, F., Xiang, R., Yi, G. X., Gong, Y., Zhao, M., et al. (2013). The *M*7.0 Lushan earthquake and the relationship with the *M*8.0 Wenchuan earthquake in Sichuan, China. *Chinese J. Geophys.* 56 (5), 1772–1873. (in Chinese). doi:10.6038/cjg20130535

Duan, H. R., Zhou, S. Y., Li, R., Chen, S. L., and Yan, Q. C. (2020). Relationship between the slip distribution of the Lushan earthquake fault and the Wenchuan earthquake fault. *Chinese J. Geophys. (in Chinese)* 63 (1), 210–222. doi:10.6038/cjg2020N0042

England, P., and Houseman, G. (1986). Finite strain calculations of continental deformation: 2. comparison with the India-Asia collision zone. *Journal of Geophysical Research Solid Earth* 91 (B3), 3664–3676. doi:10.1029/jb091ib03p03664

England, P. C., and Houseman, G. A. (1988). The mechanics of the Tibetan plateau. *Phil. Trans. R. Soc. Lod. A* 326 (1589), 301–320. doi:10.1098/rsta.1988.0089

Fu, B. H., Shi, P. L., and Zhang, Z. W. (2008). Spatial characteristics of the surface rupture by the *M*s8.0 Wenchuan earthquake using high-resolution remote sensing imagery. *Acta Geological Sinica (in Chinese)* 82 (12), 1679–1683.

Ge, W. P. (2013). Discussion on the relationship between regional landform and seismogenic structure of the MinxianZhangxian *M*s6.6 earthquake. *China earthquake engineering journal* 35 (4), 840–847. (in Chinese).

Gong, M., Xu, X. W., and Li, K. (2020). Fault geometry responsible for the initial rupture process of Wenchuan earthquake. *Chinese J. Geophys.* 63 (3), 1224–1234. (in Chinese). doi:10.6038/cjg2020N0255

Guo, R. M., Zheng, Y., and Xu, J. (2020). Stress modulation of the seismic gap between the 2008 *M*s8.0 Wenchuan earthquake and the 2013 *M*s7.0 Lushan earthquake and implications for seismic hazard. *Geophysical Journal International* 221 (3), 2113–2125. doi:10.1093/gji/ggaa143

Harrison, T. M., Copeland, P., Kidd, W. S. F., and Yin, A. (1992). Raising tibet. *Science* 255 (5052), 1663–1670. doi:10.1126/science.255.5052.1663

Huang, L. Y., Cheng, H. H., Zhang, H., Gao, Y., and Shi, Y. L. (2019). Coseismic and postseismic stress evolution caused by the 2008 Wenchuan earthquake and its effects on the 2017 *M*s7.0 Jiuzhaigou earthquake. *Chinese J. Geophys* 62 (4), 1268–1281. doi:10.6038/cjg2019L0545

Jia, K. (2020). Modeling the spatiotemporal seismicity patterns of the longmen Shan Fault zone based on the coulomb rate and state model. *Seismol. Res. lett.* 1, 275–286. –12. doi:10.1785/0220200088

Jia, K., and Zhou, S. Y. (2018). Triggering relationship in strong earthquake sequence around the Bayan Har block and its tectonic significance based on Coulomb stress changes and seismicity. *Acta Seismologica Sinica (in Chinese)* 40 (3), 291–303. doi:10.11939/jass.20170201

Jiang, Z. S., Wang, M., Wang, Y. Z., Wu, Y. Q., Che, S., Shen, Z. K., et al. (2014). GPS constrained coseismic source and slip distribution of the 2013 *M*w 6.6 Lushan, China, earthquake and its tectonic implications. *Geophys. Res. lett.* 41 (2), 407–413. doi:10.1002/2013GL058812

Jin, Z. T., Wan, Y. G., Liu, Z. C., Huang, J. C., Li, Y., and Yang, F. (2019). The static stress triggering influences of the 2017 *M*s7.0 Jiuzhaigou earthquake on neighboring areas. *Chinese J. Geophys.* 62 (4), 1282–1299. doi:10.6038/cjg2019L0675

Li, B., Xie, F. R., Huang, J. S., Xu, X. W., Guo, Q. L., Zhang, G. W., et al. (2022). *In situ* stress state and seismic hazard in the Dayi seismic gap of the Longmenshan thrust belt. *Science China (Earth Sciences)* 65 (7), 1388–1398. doi:10.1007/s11430-021-9915-4

Li, C. Y., Sun, K., Ma, J., Li, J. J., Liang, M. J., and Fang, L. H. (2022). The 2022 *M*6.8 Luding earthquake: a complicated event by faulting of the Moxi segment of the Xianshuihe fault zone. *Seismology and Geology* 44 (6), 1648–1666. doi:10.3969/j.issn.0253-4967.2022.06.017

Li, H., Wang, H., Xu, X. Q., Si, J., Pei, J., Li, T., et al. (2013). Characteristics of the fault-related rocks, fault zones and the principal slip zone in the wenchuan earthquake fault scientific drilling project hole-1 (WFSD-1). *Tectonophysics* 584, 23–42. doi:10.1016/j.tecto.2012.08.021

Li, H. B., Wang, H., Yang, G., Xu, Z. Q., Zhang, J. J., Si, J., et al. (2016). Lithological and structural characterization of the Longmenshan fault belt from the 3rd hole of the Wenchuan earthquake fault scientific drilling project (wfsd -3). *International Journal of Earth Sciences* 105 (8), 2253–2272. doi:10.1007/s00531-015-1285-9

Li, H. B., Xu, Z. Q., Wang, H., Zhang, L., He, X. L., Si, J. L., et al. (2018). Fault behavior, physical properties and seismic activity of the Wenchuan earthquake fault zone: evidences from the Wenchuan earthquake fault scientific drilling project (wfsd). *Chinese J. Geophys* 61 (5), 1680–1697. doi:10.6038/cjg2018M0257

Li, Y., Gao, Y. G., Wang, W. H., and Xu, Y. K. (2022). Benioff strain anyalysis of the Longmenshan fault zone. *China Earthquake Engineering Journal* 44 (4), 896–900. doi:10.20000/j.1000-0844.20210330001

Li, Y. Q., Jia, D., Wang, M. M., Shaw, J. H., He, J., Lin, A., et al. (2014). Structural geometry of the source region for the 2013 *M*w6.6 Lushan earthquake: implication for earthquake hazard assessment along the Longmenshan. *Earth planet. Sci. Lett.* 390, 275–286. doi:10.1016/j.epsl.2014.01.018

Li, Z. W., Liu, S. G., Chen, H. D., Liu, S., Guo, B., and Tian, X. B. (2008). Structural segmentation and zonation and differential deformation across and along the Longmen thrust belt, west Sichuan, China. *Journal of Chendu University of Technology (Science and Technology Edition)* 35 (4), 440–454.

Lin, A., Gang, R., and Bing, Y. (2012). Field evidence of rupture of the Qingchuan Fault during the 2008 *M*w7.9 Wenchuan earthquake, northeastern segment of the Longmen Shan thrust belt, China. *Tectonophysics* 522-523, 243–252. doi:10.1016/j.tecto.2011.12.012

Liu, X. M., Wu, J., Liang, C. T., Qian, Q. W., and Du, P. X. (2019). The latest seismicity characteristics and significance in Longmenshan Fault Zone. *Chinese J. Geophys* 62 (4), 1312–1322. doi:10.6038/cjg2019M0283

Liu, Y. B., and Pei, S. P. (2017). Temporal and spatial variation of *b*-value before and after Wenchuan earthquake and its tectonic implication. *Chinese J. Geophys* 60 (6), 2104–2112. doi:10.6038/cjg20170607

Lorenz, E. N. (1956). Empirical orthogonal function and statistical weather prediction. science report 1, statistical forecasting project, department of meteorology, MIT. *NTIS. AD* 110268, 1–49.

Luo, G. F., Ding, F. H., Ma, H. Q., and Yang, M. Z. (2023). Pre-quake frequency characteristics of *M*s ≥7.0 earthquake in mainland China. *Front. Earth Sci.* 10, 10–992858. doi:10.3389/feart.2022.992858

Luo, G. F., Ding, F. H., Xu, Y. C., Luo, H. Z., and Li, W. J. (2023). Strain fields of *ms* >6.0 earthquakes in menyuan, qinghai, China. *Front. Earth Sci.* 11, 1152348. doi:10.3389/feart.2023.1152348

Luo, G. F., Liu, Z. W., Luo, H. Z., and Ding, F. H. (2019). Effect of the strain field of Wenchuan 8 earthquake on the strong earthquake around the epicenter. *Progress in Geophysics (in Chinese)* 34 (3), 0908. doi:10.6038/pg2019CC0454

Luo, G. F., Ma, X. J., Ma, H. Q., and Yang, M. Z. (2015). Analysis of regional seismic energy field before Lushan *M*s7.0 earthquake. *Journal of disaster prevention and reduction (in Chinese)* 31 (1), 54–58.

Luo, G. F., Yang, M. Z., Ma, H. Q., and Xu, X. Q. (2011). Intermediate and short-term anomalies of seismic activity energy field before the Wenchuan *M*8.0 earthquake. *Earthquake(in Chinese)* 31 (3), 135–142.

Luo, G. F., Zeng, Z. W., Ma, H. Q., and Yang, M. Z. (2014). Analysis of energy field of seismic activity before the Minxian-Zhangxian *M*s6.6 Earthquake. *China earthquake engineering journal (in Chinese)* 36 (2), 314–319. doi:10.3969/j.issn.1000-0844.2014.02.0314

Luo, Y., Zhao, L., and Tian, J. H. (2019). Spatial and temporal variations of stress field in the Longmenshan fault zone after the 2008 Wenchuan, China earthquake. *Tectonophysics* 767, 228172–228213. doi:10.1016/j.tecto.2019.228172

Ma, C. H., Qian, F., and Zhang, H. M. (2021). Similation of rupture process and its influence factors of the 2013 *M*s7.0 Lushan earthquake. *Chinese J. Geophys.* 64 (1), 170–181. (in Chinese). doi:10.6038/cjg2021O0114

Mei, S. R. (1997). *General characteristics of long term evolution of seismicity before strong earthquakes in North China//Theory and method of short impending earthquake prediction*. China: Beijing Press Seismological.

Meng, W., Guo, X. Y., Li, Y. H., Han, L. B., and Zhang, C. Y. (2022). Tectonic stress field and dynamic characteristics in the northeastern margin of the Tibetan Plateau. *Chinese J. Geophys.* 65 (9), 3229–3251. (in Chinese). doi:10.6038/cjg2022P0236

Molnar, P., and Tapponnier, P. (1975). Cenozoic Tectonics of Asia: effects of a Continental Collision: features of recent continental tectonics in Asia can be interpreted as results of the India-Eurasia collision. *Science* 189 (4201), 419–426. doi:10.1126/science.189.4201.419

Neha, and Pasari, S. (2022). A review of empirical orthogonal function (eof) with an emphasis on the co-seismic crustal deformation analysis. *Nat. Hazards.* 110, 29–56. doi:10.1007/s11069-021-04967-4

Obukhov, A. M. (1960). The statistically orthogonal expansion of empirical functions. bulletin of the academy of sciences of the USSR. *Geophys Ser* 1, 288–291.

Shan, X. J., Qu, C. Y., Gong, W. Y., Zhao, D. Z., Zhang, Y. F., Zhang, G. F., et al. (2017). Coseismic deformation field of the Jiuzhaigou *Ms*7.0 earthquake form Sentinel-1A InSAR data and fault slip inversion. *Chinese J. Geophys. (in Chinese)* 60 (12), 4527–4536. doi:10.6038/cjg20171201

Shi, Y. L., and Cao, J. L. (2010). Some aspects in static stress change calculation case study on Wenchuan earthquake. *Chinese Journal of Geophysics (in Chinese)* 51 (1), 102–110. doi:10.3969/j.issn.0001-5733.2010.01.011

Teng, J. W., Pi, J. L., Yang, H., Yan, Y. F., Zhang, Y. Q., Yuan, X. M., et al. (2014). Wenchuan-Yingxiu *Ms*8.0 earthquake seismogenic fault and deep dynamic response. *Chinese J. Geophys* 57 (2), 392–403. doi:10.6038/cjg20140604

Tiampo, K. F., and Shcherbakov, R. (2012). Seismicity-based earthquake forecasting techniques: ten years of progress. *Tectonophysics* 522–523, 89–121. doi:10.1016/j.tecto.2011.08.019

Toda, S., Lin, J., Meghraoui, M., and Stein, R. (2008). 12 May 2008 *M*7.9 Wenchuan, China, earthquake calculated to increase failure stress and seismicity rate on three major fault systems, *Geophys. Res. Lett.* 35, 1–6. doi:10.1029/2008GL034903

Wan, Y. G. (2020). Simulation on relationship between stress and mechanisms of earthquake. *Chinese Journal of Geophysics* 63 (6), 2281–2296. doi:10.6038/cjg2023Q0093

Wan, Y. G., Shen, Z. K., Sheng, S. Z., and Xu, X. F. (2009). The influence of 2008 Wenchuan earthquake on surrounding faults. *Acta Seismologica Sinica (in Chinese)* 31 (2), 128–139.

Wan, Y. R., Shen, Z. K., Bvrgmann, R., Sun, J. B., and Wang, M. (2017). Fault geometry and slip distribution of the 2008 *M*w7.9 Wenchuan, China earthquake, inferred from GPS and InSAR measurements. *Geophys. J. Int.* 208 (2), 748–766. doi:10.1093/gji/ggw421

Wang, J. J., Xu, C. J., Freymueller, J. T., Li, Z. H., and Shen, W. B. (2014). Sensitivity of coulomb stress change to the parameters of the coulomb failure model: a case study using the 2008 *M*w7.9 Wenchuan earthquake. *J. Geophys. Res. Solid Earth.* 119 (4), 3371–3392. doi:10.1002/2012jb009860

Wang, W. M., Hao, J. L., and Yao, Z. X. (2013). Preliminary result for rupture process of Apr. 20,2013,Lushan earthquake,Sichuan, China. *Chinese J. Geophys.* 56 (4), 1412–1417. (in Chinese). doi:10.6038/cjg20130436

Wang, X. F., Xiao, J., Xu, H. H., and He, J. K. (2016). Dynamic responses of the Xianshuihe and Longmenshan fault zones to regional tectonic loading. *Chinese J. Geophys. (in Chinese)* 59 (4), 1403–1413. doi:10.6038/cjg20160421

Wang, X. S., Lu, J., Xie, Z. J., Long, F., Zhao, X. Y., and Zheng, Y. (2015). Focal mechanisms and tectonic stress field in the north-south seismic Belt of China. *Chinese J. Geophys* 58 (11), 4149–4162. (in Chinese). doi:10.6038/cjg20151122

Wang, Y. Z., Wang, F., Wang, M., Shen, Z. K., and Wan, Y. G. (2014). Coulomb stress change and evolution induced by the 2008 Wenchuan earthquake and its delayed triggering of the 2013 *M*w 6.6 Lushan earthquake. *Seismol. Res. Lett.* 85 (1), 52–59. doi:10.1785/0220130111

Wang, Z., Wang, X. B., Huang, R. Q., and Liu, G. N. (2017). Deep structre imaging of multi-geophysical parameters and seismogenesis in the Longmenshan fault zone. *Chinese J. Geophys.* 60 (6), 2068–2079. (in Chinese). doi:10.6038/cjg20170604

Wu, Y. Q., Jiang, Z. S., Zhao, J., Liu, X. X., Wei, W. X., Liu, Q., et al. (2015). Crustal deformation before the 2008 Wenchuan *Ms*8.0 earthquanke studied using GPS data. *J. Geodyn.* 85, 11–23. doi:10.1016/j.jog.2014.12.002

Xie, J. J., Li, X. J., Wen, Z. P., and Zou, B. (2018). Variation of near-fault strong ground motion with directions during the 2013 Lushan *Ms*7.0 earthquake. *Chinese J. Geophys. (in Chinese)* 61 (4), 1266–1280. doi:10.6038/cjg2018K0686

Xu, X. W., Chen, G. H., Wang, Q. X., Chen, L. C., Ren, Z. S., and Xu, C. (2017). Discussion on seismogenic structure of Jiuzhaigou earthquake and its implication for current strain state in southeastern Qinghai-Tibet Plateau. *Chinese J. Geophys. (in Chinese)* 60 (10), 4018–4026. doi:10.6038/cjg20171028

Xu, X. W., Chen, G. H., Yu, G. H., Sun, X. J., Tan, X. B., and Chen, L. C. (2010). Reevaluation of surface rupture parameters of the 5·12 Wenchuan earthquake and its tectonic implication for Tibetan uplift. *Chinese Journal of Geophysics (in Chinese)* 53 (10), 2321–2336. doi:10.3969/j.issn.0001-5733.2010.10.006

Xu, X. W., Wen, X. Z., Han, Z. J., Chen, G. H., Li, C. Y., Zhen, W. J., et al. (2013). Lushan *Ms*7.0 earthquake: a blind reserve-fault event. *Chinese Sci. Bull.* 58 (28), 3437–3443. doi:10.1007/s11434–013–5999–4

Xu, X. W., Wen, X. Z., Ye, J. Q., Ma, B. Q., Chen, J., Zhou, R. J., et al. (2008). The *M*s8.0 Wenchuan earthquake surface ruptures and its seismogenic structure. *Seismology and Geology (in Chinese)* 30 (3), 597–629.

Xu, X. W., Wen, X. Z., Yu, G. H., Chen, G. H., Klinger, Y., Hubbard, J., et al. (2009). Coseismal reverse and oblique-slip surface faulting generated by the 2008 *M*w7.9 Wenchuan earthquake, China. *Grology* 37 (6), 515–518. doi:10.1130/G25462A.1

Xu, Z. Q., Wu, Z. L., Li, H. B., and Li, L. (2018). The most rapid respond to a large earthquake—the Wenchuan earthquake fault scientific drilling project. *Chinese J. Geophys.* 61 (5), 1666–1679. doi:10.6038/cjg2018M0256

Yan, Z. K., Li, Y., Zhao, G. H., Zhou, R. J., Li, J. B., Zhang, W., et al. (2014). The relationship between Lushan earthquake and Wenchuan earthquake by segmentation of geology and geomorphology of LongmenShan. *Chinese Journal of Nature (in Chinese)* 36 (1), 51–58.

Yang, M. Z., and Ma, H. Q. (2011). Variation of energy field of Longmenshan fault zone before the Wenchuan *Ms*8.0 earthquake. *Earthquake Research in China (in Chinese)* 27 (3), 260–267.

Yang, M. Z., and Ma, H. Q. (2012). Analysis of regional seismic energy field before Wenchuan *Ms*8.0 earthquake. *Progress in Geophysics (in Chinese)* 27 (3), 872–877. doi:10.6038/j.issn.1004-2903.2012.03.006

Yang, M. Z., and Ma, H. Q. (2016). Seismic active field theory and anomaly analysis method. *Beijing Press Seismological*, 23–39.

Yang, M. Z., Ma, H. Q., Luo, G. F., and Xu, X. Q. (2017). Research on the seismic strain field before strong earthquakes above *M*6 in Chinese mainland. *Chinese J. Geophys. (in Chinese)* 60 (10), 3804–3814. doi:10.6038/cjg20171010

Yang, M. Z., and Zhao, W. M. (2004). Statistical analysis of seismic activity energy field in Ningxia and its adjacent areas. *Journal of Earthquake (in Chinese)* 26 (5), 571–577.

Yang, X. P., Jiang, P., Song, F. M., Liang, X. H., and Chen, X. C. (1999). The evidence of the south Longmenshan Fault zones cuting late Quaternary stratum. *Seismology and Geology (in Chinese)* 21 (4), 341–345.

Yang, Y. H., Zhang, X. M., Hua, Q., Sou, L. N., Feng, C. J., Qiu, Y. R., et al. (2021). Segmentation characteristics of the Longmenshan fault—constrained from dense focal mechanism data. *Chinese J. Geophys.* 64 (4), 1181–1205. doi:10.6038/cjg2021O0286

Ye, Q. D., Ding, Z. F., Wang, S. W., Yu, D. X., and Zhen, C. (2017). Determining the source parameters of the micro earthquakes near the third borehole of the Wenchuan Earthquake Fault Scientific (wfsd-3) and its implications. *Chinese J. Geophys. (in Chinese)* 60 (7), 2716–2732. doi:10.6038/cjg20170718

Yi, G. X., Long, F., Liang, M. J., Zhang, H. P., Zhao, M., and Ye, Y. Q. (2017). Focal mechanism solution and seismogenic structure of the 8 August 2017 Jiuzhaigou (*M*7.0) earthquake and its aftershocks, northern Sichuan. *Chinese J. Geophys.* 60 (10), 4083–4097. doi:10.6038/cjg20171033

Yi, G. X., Long, F., Vallage, A., Klinger, Y., Liang, M. J., and Wang, S. W. (2016). Focal mechanism and tectonic deformation in the seismogenic area of the 2013 Lushan earthquake sequence southwestern China. *Chinese J. Geophys.* 59 (10), 3711–3731. doi:10.6038/cjg20161017

Yi, G. X., Long, F., Wen, X. Z., Liang, M. J., and Wang, S. W. (2015). Seismogenic structure of the *M*6.3 kangding earthquake sequence on 22 nov. 2014, southwestern China. *Chinese J. Geophys.* 58 (4), 1205–1219. doi:10.6038/cjg20150410

Yi, G. X., Long, F., and Zhang, Z. W. (2012). Spatial and temporal variation of focal mechanisms for aftershocks of the 2008 *Ms*8.0 Wenchuan earthquake. *Chinese J. Geophys.* 55 (4), 1213–1227. doi:10.6038/j.issn.0001-5733.2012.04.017

Yi, G. X., Wen, X. Z., Xin, H., Qiao, H. Z., Wang, S. W., and Gong, Y. (2013). Stress state and major earthquake risk on the southern segment of the Longmen Shan fault zone. *Chinese Journal of geophysics Chinese edition* 56 (4), 1112–1120. doi:10.6038/cjg20130407

Zhang, P. Z., Wen, X. Z., Shen, Z. K., and Chen, J. H. (2008). Oblique, high-angle, listric-reverse faulting and associated development of strain: the Wenchuan earthquake of May 12, 2008, Sichuan, China. *Annu. Rev.Earth Planet* 38, 353–382. doi:10.1146/annurev-earth-040809-152602

Zhang, P. Z., Wen, X. Z., Xu, X. W., Zhang, P., Wen, X., Huang, Y., et al. (2009). Multi-unit combination model of the 2008 Wenchuan magnitude 8.0 earthquake. *Chin. Sci. Bull. (in Chinese)* 54 (7), 944–953. doi:10.1360/csb2009-54-7-944

Zhao, B., Gao, Y., Huang, Z. B., Zhao, X., and Li, D. (2013). Double difference relocation, focal mechanism and stress inversion of Lushan *Ms*7.0 earthquake sequence. *Chinese J. Geophys. (in Chinese)* 56 (10), 3385–3395. doi:10.6038/cjg20131014

Zheng, T., Ding, Z. F., Chang, L. J., Zhen, C., Zhang, H., and Li, D. F. (2017). *S*-ware slitting in upper crust near the scientific drilling wfsd-3 at the Wenchuan earthquake fault zone. *Chinese J. Geophys* 60 (5), 1690–1702. (in Chinese). doi:10.6038/cjg20170507